

## 4.5 Parametric Spectral Estimation

The methods of the previous section lead to what is generally referred to as *non-parametric spectral estimators* because no assumption is made about the parametric form of the spectral density. In [Property 4.4](#), we exhibited the spectrum of an ARMA process and we might consider basing a spectral estimator on this function, substituting the parameter estimates from an ARMA( $p, q$ ) fit on the data into the formula for the spectral density  $f_x(\omega)$  given in (4.23). Such an estimator is called a parametric spectral estimator. For convenience, a parametric spectral estimator is obtained by fitting an AR( $p$ ) to the data, where the order  $p$  is determined by one of the model selection criteria, such as AIC, AICc, and BIC, defined in (2.15)–(2.17). Parametric autoregressive spectral estimators will often have superior resolution in problems when several closely spaced narrow spectral peaks are present and are preferred by engineers for a broad variety of problems (see Kay, 1988). The development of autoregressive spectral estimators has been summarized by Parzen (1983).

If  $\hat{\phi}_1, \hat{\phi}_2, \dots, \hat{\phi}_p$  and  $\hat{\sigma}_w^2$  are the estimates from an AR( $p$ ) fit to  $x_t$ , then based on [Property 4.4](#), a parametric spectral estimate of  $f_x(\omega)$  is attained by substituting these estimates into (4.23), that is,

$$\hat{f}_x(\omega) = \frac{\hat{\sigma}_w^2}{|\hat{\phi}(e^{-2\pi i\omega})|^2}, \quad (4.82)$$

The asymptotic distribution of the autoregressive spectral estimator has been obtained by Berk (1974) under the conditions  $p \rightarrow \infty, p^3/n \rightarrow 0$  as  $p, n \rightarrow \infty$ , which may be too severe for most applications. The limiting results imply a confidence interval of the form

$$\frac{\hat{f}_x(\omega)}{(1 + Cz_{\alpha/2})} \leq f_x(\omega) \leq \frac{\hat{f}_x(\omega)}{(1 - Cz_{\alpha/2})}, \quad (4.84)$$

where  $C = \sqrt{2p/n}$  and  $z_{\alpha/2}$  is the ordinate corresponding to the upper  $\alpha/2$  probability of the standard normal distribution. If the sampling distribution is to be checked, we suggest applying [the bootstrap estimator](#) to get the sampling distribution of  $\hat{f}_x(\omega)$  using a procedure similar to the one used for  $p = 1$  in [Example 3.36](#). An alternative for higher order autoregressive series is to put the AR( $p$ ) in state-space form and use the bootstrap procedure discussed in [Section 6.7](#).

An interesting fact about rational spectra of the form (4.23) is that any spectral density can be approximated, arbitrarily close, by the spectrum of an AR process.

**Property 4.7 AR Spectral Approximation**

Let  $g(\omega)$  be the spectral density of a stationary process. Then, given  $\epsilon > 0$ , there is a time series with the representation

$$x_t = \sum_{k=1}^p \phi_k x_{t-k} + w_t$$

where  $w_t$  is white noise with variance  $\sigma_w^2$ , such that

$$|f_x(\omega) - g(\omega)| < \epsilon \quad \text{for all } \omega \in [-1/2, 1/2].$$

Moreover,  $p$  is finite and the roots of  $\phi(z) = 1 - \sum_{k=1}^p \phi_k z^k$  are outside the unit circle.

**Example 4.18 Autoregressive Spectral Estimator for SOI**

Consider obtaining results comparable to the nonparametric estimators shown in Figure 4.7 for the SOI series. Fitting successively higher order AR( $p$ ) models for  $p = 1, 2, \dots, 30$  yields a minimum BIC and a minimum AIC at  $p = 15$  as shown in Figure 4.13. We can see from Figure 4.13 that BIC is very definite about which model it chooses; that is, the minimum BIC is very distinct. On the other hand, it is not clear what is going to happen with AIC; that is, the minimum is not so clear, and there is some concern that AIC will start decreasing after  $p = 30$ . Minimum AICc selects the  $p = 15$  model, but suffers from the same uncertainty as AIC. The spectrum is shown in Figure 4.14, and we note the strong peaks near the four year

and one year cycles as in the nonparametric estimates obtained in Section 4.4. In addition, the harmonics of the yearly period are evident in the estimated spectrum.

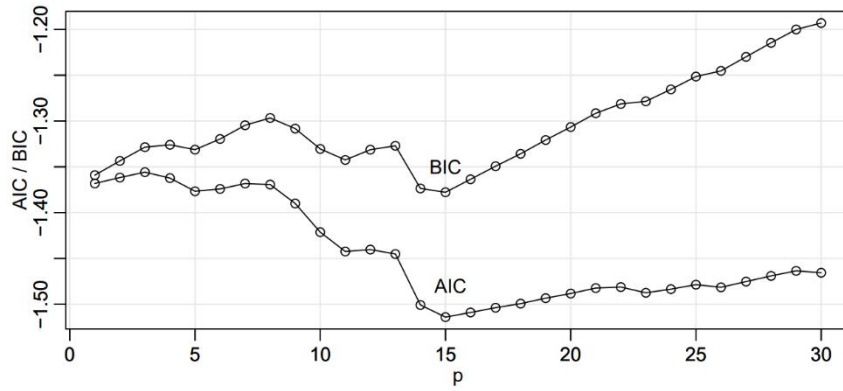


**Fig. 4.13.** Model selection criteria AIC and BIC as a function of order  $p$  for autoregressive models fitted to the SOI series.

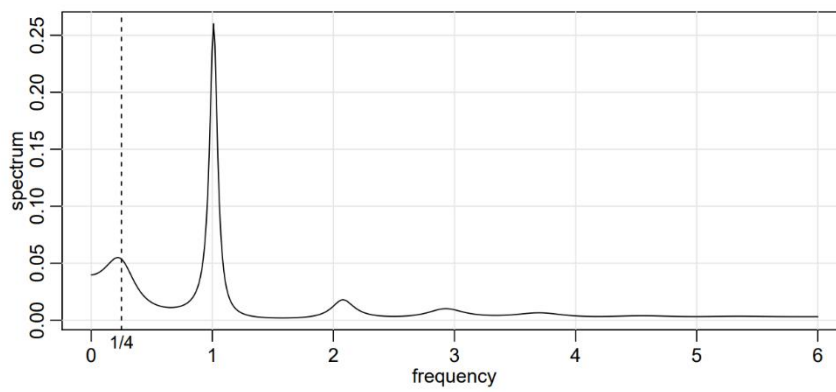


**Fig. 4.14.** Autoregressive spectral estimator for the SOI series using the AR(15) model selected by AIC, AICc, and BIC.

## 4.6 Multiple Series and Cross-Spectra

The notion of analyzing frequency fluctuations using classical statistical ideas extends to the case in which there are several jointly stationary series, for example,  $x_t$  and  $y_t$ . In this case, we can introduce the idea of a correlation indexed by frequency, called the *coherence*. The results in Section C.2 imply the covariance function

$$\gamma_{xy}(h) = E[(x_{t+h} - \mu_x)(y_t - \mu_y)]$$

has the representation

$$\gamma_{xy}(h) = \int_{-\frac{1}{2}}^{\frac{1}{2}} f_{xy}(\omega) e^{2\pi i \omega h} d\omega \quad h = 0, \pm 1, \pm 2, \dots, \quad (4.86)$$

where the *cross-spectrum* is defined as the Fourier transform

$$f_{xy}(\omega) = \sum_{h=-\infty}^{\infty} \gamma_{xy}(h) e^{-2\pi i \omega h} \quad -1/2 \leq \omega \leq 1/2, \quad (4.87)$$

assuming that the cross-covariance function is absolutely summable, as was the case for the autocovariance. The cross-spectrum is generally a complex-valued function, and it is often written as

$$f_{xy}(\omega) = c_{xy}(\omega) - i q_{xy}(\omega), \quad (4.88)$$

where

$$c_{xy}(\omega) = \sum_{h=-\infty}^{\infty} \gamma_{xy}(h) \cos(2\pi \omega h) \quad (4.89)$$

and

$$q_{xy}(\omega) = \sum_{h=-\infty}^{\infty} \gamma_{xy}(h) \sin(2\pi \omega h) \quad (4.90)$$

are defined as the *cospectrum* and *quadspectrum*, respectively. Because of the relationship  $\gamma_{yx}(h) = \gamma_{xy}(-h)$ , it follows, by substituting into (4.87) and rearranging, that

$$f_{yx}(\omega) = f_{xy}^*(\omega), \quad (4.91)$$

with  $*$  denoting conjugation. This result, in turn, implies that the cospectrum and quadspectrum satisfy

$$c_{yx}(\omega) = c_{xy}(\omega) \quad (4.92)$$

and

$$q_{yx}(\omega) = -q_{xy}(\omega). \quad (4.93)$$

An important example of the application of the cross-spectrum is to the problem of predicting an output series  $y_t$  from some input series  $x_t$  through a linear filter relation such as the three-point moving average considered below. A measure of the strength of such a relation is the *squared coherence* function, defined as

$$\rho_{y \cdot x}^2(\omega) = \frac{|f_{yx}(\omega)|^2}{f_{xx}(\omega)f_{yy}(\omega)}, \quad (4.94)$$

where  $f_{xx}(\omega)$  and  $f_{yy}(\omega)$  are the individual spectra of the  $x_t$  and  $y_t$  series, respectively. Although we consider a more general form of this that applies to multiple inputs later, it is instructive to display the single input case as (4.94) to emphasize the analogy with conventional squared correlation, which takes the form

$$\rho_{yx}^2 = \frac{\sigma_{yx}^2}{\sigma_x^2 \sigma_y^2},$$

for random variables with variances  $\sigma_x^2$  and  $\sigma_y^2$  and covariance  $\sigma_{yx} = \sigma_{xy}$ . This motivates the interpretation of squared coherence and the squared correlation between two time series at frequency  $\omega$ .

#### Example 4.19 Three-Point Moving Average

As a simple example, we compute the cross-spectrum between  $x_t$  and the three-point moving average  $y_t = (x_{t-1} + x_t + x_{t+1})/3$ , where  $x_t$  is a stationary input process with spectral density  $f_{xx}(\omega)$ . First,

$$\begin{aligned} \gamma_{xy}(h) &= \text{cov}(x_{t+h}, y_t) = \frac{1}{3} \text{cov}(x_{t+h}, x_{t-1} + x_t + x_{t+1}) \\ &= \frac{1}{3} [\gamma_{xx}(h+1) + \gamma_{xx}(h) + \gamma_{xx}(h-1)] \\ &= \frac{1}{3} \int_{-\frac{1}{2}}^{\frac{1}{2}} (e^{2\pi i \omega} + 1 + e^{-2\pi i \omega}) e^{2\pi i \omega h} f_{xx}(\omega) d\omega \\ &= \frac{1}{3} \int_{-\frac{1}{2}}^{\frac{1}{2}} [1 + 2 \cos(2\pi \omega)] f_{xx}(\omega) e^{2\pi i \omega h} d\omega, \end{aligned}$$

where we have used (4.16). Using the uniqueness of the Fourier transform, we argue from the spectral representation (4.86) that

$$f_{xy}(\omega) = \frac{1}{3} [1 + 2 \cos(2\pi \omega)] f_{xx}(\omega)$$

so that the cross-spectrum is real in this case. Using [Property 4.3](#), the spectral density of  $y_t$  is

$$f_{yy}(\omega) = \frac{1}{9} |e^{2\pi i \omega} + 1 + e^{-2\pi i \omega}|^2 f_{xx}(\omega) = \frac{1}{9} [1 + 2 \cos(2\pi \omega)]^2 f_{xx}(\omega).$$

Substituting into (4.94) yields,

$$\rho_{y \cdot x}^2(\omega) = \frac{\left| \frac{1}{3} [1 + 2 \cos(2\pi \omega)] f_{xx}(\omega) \right|^2}{f_{xx}(\omega) \cdot \frac{1}{9} [1 + 2 \cos(2\pi \omega)]^2 f_{xx}(\omega)} = 1;$$

that is, the squared coherence between  $x_t$  and  $y_t$  is unity over all frequencies. This is a characteristic inherited by more general linear filters; see [Problem 4.30](#). However, if some noise is added to the three-point moving average, the coherence is not unity; these kinds of models will be considered in detail later.



**Property 4.8 Spectral Representation of a Vector Stationary Process**

If  $x_t = (x_{t1}, x_{t2}, \dots, x_{tp})'$  is a  $p \times 1$  stationary process with autocovariance matrix  $\Gamma(h) = E[(x_{t+h} - \mu)(x_t - \mu)'] = \{\gamma_{jk}(h)\}$  satisfying

$$\sum_{h=-\infty}^{\infty} |\gamma_{jk}(h)| < \infty \quad (4.95)$$

for all  $j, k = 1, \dots, p$ , then  $\Gamma(h)$  has the representation

$$\Gamma(h) = \int_{-\frac{1}{2}}^{\frac{1}{2}} e^{2\pi i \omega h} f(\omega) d\omega \quad h = 0, \pm 1, \pm 2, \dots, \quad (4.96)$$

as the inverse transform of the spectral density matrix,  $f(\omega) = \{f_{jk}(\omega)\}$ , for  $j, k = 1, \dots, p$ . The matrix  $f(\omega)$  has the representation

$$f(\omega) = \sum_{h=-\infty}^{\infty} \Gamma(h) e^{-2\pi i \omega h} \quad -1/2 \leq \omega \leq 1/2. \quad (4.97)$$

The spectral matrix  $f(\omega)$  is Hermitian,  $f(\omega) = f^*(\omega)$ , where  $*$  means to conjugate and transpose.

**Example 4.20 Spectral Matrix of a Bivariate Process**

Consider a jointly stationary bivariate process  $(x_t, y_t)$ . We arrange the autocovariances in the matrix

$$\Gamma(h) = \begin{pmatrix} \gamma_{xx}(h) & \gamma_{xy}(h) \\ \gamma_{yx}(h) & \gamma_{yy}(h) \end{pmatrix}.$$

The spectral matrix would be given by

$$f(\omega) = \begin{pmatrix} f_{xx}(\omega) & f_{xy}(\omega) \\ f_{yx}(\omega) & f_{yy}(\omega) \end{pmatrix},$$

where the Fourier transform (4.96) and (4.97) relate the autocovariance and spectral matrices.

The extension of spectral estimation to vector series is fairly obvious. For the vector series  $x_t = (x_{t1}, x_{t2}, \dots, x_{tp})'$ , we may use the vector of DFTs, say  $d(\omega_j) = (d_1(\omega_j), d_2(\omega_j), \dots, d_p(\omega_j))'$ , and estimate the spectral matrix by

$$\bar{f}(\omega) = L^{-1} \sum_{k=-m}^m I(\omega_j + k/n) \quad (4.98)$$

where now

$$I(\omega_j) = d(\omega_j) d^*(\omega_j) \quad (4.99)$$

is a  $p \times p$  complex matrix. The series may be tapered before the DFT is taken in (4.98) and we can use weighted estimation,

$$\hat{f}(\omega) = \sum_{k=-m}^m h_k I(\omega_j + k/n) \quad (4.100)$$

where  $\{h_k\}$  are weights as defined in (4.64). The estimate of squared coherence between two series,  $y_t$  and  $x_t$  is

$$\hat{\rho}_{y \cdot x}^2(\omega) = \frac{|\hat{f}_{yx}(\omega)|^2}{\hat{f}_{xx}(\omega) \hat{f}_{yy}(\omega)}. \quad (4.101)$$

If the spectral estimates in (4.101) are obtained using equal weights, we will write  $\bar{\rho}_{y \cdot x}^2(\omega)$  for the estimate.

Under general conditions, if  $\rho_{y \cdot x}^2(\omega) > 0$  then

$$|\hat{\rho}_{y \cdot x}(\omega)| \sim AN \left( |\rho_{y \cdot x}(\omega)|, (1 - \rho_{y \cdot x}^2(\omega))^2 / 2L_h \right) \quad (4.102)$$

where  $L_h$  is defined in (4.65); the details of this result may be found in Brockwell and Davis (1991, Ch 11). We may use (4.102) to obtain approximate confidence intervals for the squared coherence,  $\rho_{y \cdot x}^2(\omega)$ .

We may also test the null hypothesis that  $\rho_{y \cdot x}^2(\omega) = 0$  if we use  $\bar{\rho}_{y \cdot x}^2(\omega)$  for the estimate with  $L > 1$ ,<sup>4.11</sup> that is,

$$\bar{\rho}_{y \cdot x}^2(\omega) = \frac{|\bar{f}_{yx}(\omega)|^2}{\bar{f}_{xx}(\omega) \bar{f}_{yy}(\omega)}. \quad (4.103)$$

In this case, under the null hypothesis, the statistic

$$F = \frac{\bar{\rho}_{y \cdot x}^2(\omega)}{(1 - \bar{\rho}_{y \cdot x}^2(\omega))} (L - 1) \quad (4.104)$$

has an approximate  $F$ -distribution with 2 and  $2L - 2$  degrees of freedom. When the series have been extended to length  $n'$ , we replace  $2L - 2$  by  $df - 2$ , where  $df$  is defined in (4.60). Solving (4.104) for a particular significance level  $\alpha$  leads to

<sup>4.11</sup> If  $L = 1$  then  $\bar{\rho}_{y \cdot x}^2(\omega) \equiv 1$ .

$$C_\alpha = \frac{F_{2, 2L-2}(\alpha)}{L - 1 + F_{2, 2L-2}(\alpha)} \quad (4.105)$$

as the approximate value that must be exceeded for the original squared coherence to be able to reject  $\rho_{y \cdot x}^2(\omega) = 0$  at an a priori specified frequency.

#### Example 4.21 Coherence Between SOI and Recruitment

Figure 4.15 shows the squared coherence between the SOI and Recruitment series over a wider band than was used for the spectrum. In this case, we used  $L = 19$ ,  $df = 2(19)(453/480) \approx 36$  and  $F_{2,df-2}(.001) \approx 8.53$  at the significance level  $\alpha = .001$ . Hence, we may reject the hypothesis of no coherence for values of  $\tilde{\rho}_{y,x}^2(\omega)$  that exceed  $C_{.001} = .32$ . We emphasize that this method is crude because, in addition to the fact that the  $F$ -statistic is approximate, we are examining the squared coherence across all frequencies with the Bonferroni inequality, (4.63), in mind. Figure 4.15 also exhibits confidence bands as part of the R plotting routine. We emphasize that these bands are only valid for  $\omega$  where  $\rho_{y,x}^2(\omega) > 0$ .

In this case, the two series are obviously strongly coherent at the annual seasonal frequency. The series are also strongly coherent at lower frequencies that may be attributed to the El Niño cycle, which we claimed had a 3 to 7 year period. The peak in the coherence, however, occurs closer to the 9 year cycle. Other frequencies are also coherent, although the strong coherence is less impressive because the underlying power spectrum at these higher frequencies is fairly small. Finally, we note that the coherence is persistent at the seasonal harmonic frequencies.

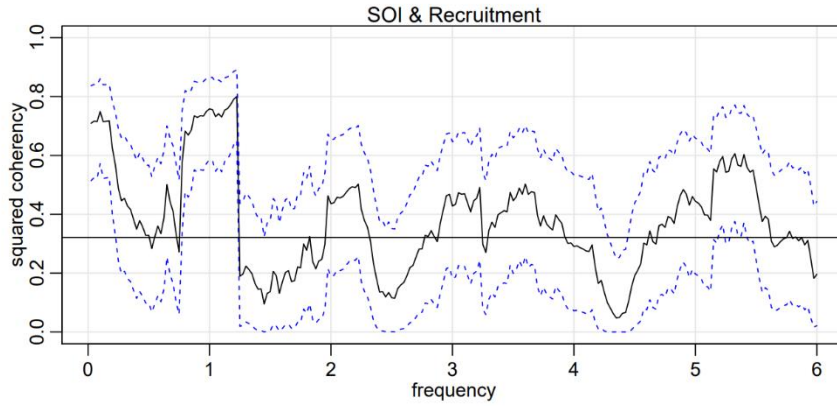


**Fig. 4.15.** Squared coherency between the SOI and Recruitment series;  $L = 19$ ,  $n = 453$ ,  $n' = 480$ , and  $\alpha = .001$ . The horizontal line is  $C_{.001}$ .